

1                   **Rapid glaciation and a two-step sea-level plunge into**

2                                   **The Last Glacial Maximum**

3

4   Yusuke Yokoyama<sup>1,2,3\*</sup>, Tezer M Esat<sup>4,5</sup>, William G Thompson<sup>6</sup>, Alexander L Thomas<sup>7</sup>, Jody

5   M. Webster<sup>8</sup>, Yosuke Miyairi<sup>1</sup>, Chikako Sawada<sup>1</sup>, Takahiro Aze<sup>1</sup> Hiroyuki Matsuzaki<sup>9</sup>, Jun'ichi

6   Okuno<sup>10</sup>, Stewart Fallon<sup>4</sup>, Juan-Carlos Braga<sup>11</sup>, Marc Humblet<sup>12</sup>, Yasufumi Iryu<sup>13</sup>, Donald C

7   Potts<sup>14</sup>, Kazuhiko Fujita<sup>15</sup>, Atsushi Suzuki<sup>16</sup>, Hironobu Kan<sup>17</sup>

8

9   <sup>1</sup>. Atmosphere and Ocean Research Institute, University of Tokyo, Japan. <sup>2</sup>. Department of Earth  
10 and Planetary Science, Graduate School of Science, University of Tokyo, Japan. <sup>3</sup>. Japan  
11 Agency for Marine-Earth Science and Technology, Yokosuka, Japan. <sup>4</sup>. Research School of  
12 Earth Sciences, Australian National University, Canberra, ACT, Australia. <sup>5</sup>. Research School of  
13 Physics and Engineering, Australian National University, Canberra, ACT, Australia. <sup>6</sup>. Woods  
14 Hole Oceanographic Institution, Woods Hole, MA, United States. <sup>7</sup>. University of Edinburgh,  
15 Edinburgh, United Kingdom. <sup>8</sup>. University of Sydney, Sydney, NSW, Australia. <sup>9</sup>. University  
16 Museum, University of Tokyo, Japan. <sup>10</sup>. National Institute of Polar Research, Japan. <sup>11</sup>.

17 Universidad de Granada, Granada, Spain. <sup>12</sup> Nagoya University, Nagoya, Japan. <sup>13</sup> Tohoku  
18 University, Sendai, Japan. <sup>14</sup> University of California Santa Cruz, Santa Cruz, CA, United  
19 States. <sup>15</sup> University of Ryukyu, Japan. <sup>16</sup> Geological Survey of Japan, Japan <sup>17</sup> Kyushu  
20 University, Japan.

21 **The ~10 thousand year-long Last Glacial Maximum (LGM), prior to the termination of**  
22 **the last ice age, was the coldest period in Earth's recent climate history<sup>1</sup>. The LGM began**  
23 **when sea-levels abruptly dropped by ~40 m at ~31 ka<sup>2</sup> and was followed by ~10,000 years**  
24 **of rapid deglaciation into the Holocene<sup>1</sup>. The LGM tropical sea surface temperatures**  
25 **(SST) were 3-5 °C colder and atmospheric greenhouse gasses were lower than today<sup>3,4</sup>.**  
26 **The masses of the melting polar ice sheets, the change in ocean volume and hence the sea**  
27 **level is a primary constraint for climate models constructed to describe the**  
28 **LGM-Holocene transition. We have recovered fossil corals and coralline algae from the**  
29 **shelf edge of the Great Barrier Reef (GBR). Radiometric dating of well-characterised**  
30 **biological assemblages enabled LGM sea-levels to be resolved in exceptional detail where,**  
31 **previously, there was a dearth of data. The resulting local, relative sea level (RSL) record**  
32 **shows a hitherto unrecognised very rapid, ~20 m sea-level drop between 22-21.5 ka to a**

33 **RSL of -118 m after which the sea-level rises at a rate of ~3.5 mm/yr for a short, ~4 ky,**  
34 **period. The rise in sea-level is consistent with the warming previously observed at 19 ka<sup>1,5</sup>,**  
35 **but here it occurs following a very rapid increase in global ice volumes. The detailed**  
36 **structure of our new record is robust as the GBR is remote from former ice sheets and**  
37 **tectonic activity. Local sea levels can be influenced by the Earth's response to regional**  
38 **changes in ice and water loadings and may significantly differ from global mean sea levels**  
39 **(GMSL). We have employed glacio-isostatic (GIA) models to derive mean global sea levels,**  
40 **throughout the LGM, which culminate in sea-level lows of -125 to -130 m.**

41 The LGM to Holocene sea level rise was at times episodic and stimulated particular patterns in  
42 coral reef growth and evolution. Estimates of the maximum volume of excess ice and amount of  
43 water that contributed to the change in the corresponding GMSL was originally based on the  
44 stratigraphy of radiocarbon and U-series dated corals from Barbados<sup>6,7</sup>. Data from radiocarbon  
45 dated micro and macro fossils also helped define LGM paleo-shorelines from Sunda Shelf in  
46 South China Sea<sup>8</sup> and Bonaparte Gulf of Northern Australia<sup>5,9</sup>. However, large uncertainties  
47 remain in local relative sea level data and in GIA model inputs, such as ice histories and Earth

48 rheology. These are needed in estimating the bounds of past and future global mean sea levels  
49 which, for the LGM, range from 115 m to 135 m<sup>2,10</sup>.

50 Precise and accurate sea level histories, often derived from dating of fossil corals and algae, are  
51 important. Coastal shelf geometry and location of land-bridges and islands at the LGM have a  
52 bearing on probable human migration routes and impact the ecological and species diversity, for  
53 example, of endemic flowering plants on islands that had complex, dynamic histories and  
54 covered a larger area during the LGM<sup>11</sup>. Sea-levels vary with polar ice volumes and the extent  
55 of LGM ice-sheets can affect atmospheric pressure patterns and alter the salinity of oceans  
56 causing circulation changes<sup>4</sup>.

57 Fossil coral and coralline algae deposits of the LGM-Holocene period at the GBR are below  
58 present sea level and were drilled during the Integrated Ocean Drilling Program (IODP)  
59 Expedition 325 in 2010<sup>12</sup> (Fig.1). Corals and coralline algae were recovered from 34 holes, over  
60 two transects 500 km apart, at Hydrographers Passage (HYD-01C) and Noggin Pass  
61 (NOG-01B; Fig.1). Depths, up to 150 m below sea level were reached to access the full LGM  
62 period<sup>12</sup>. Selected, well characterized, samples were dated by U-series (coral) and accelerator  
63 based radiocarbon (coral and algae) methods (Extended Data Table 1). Sea level depth

64 uncertainties depend on the paleo-habitat depth range of particular coral and algae species and  
65 were conservatively assessed in conjunction with associated algal crust thickness, vermetid  
66 gastropods and by benthic foraminiferal assemblages<sup>12,13</sup> (Figs. 2, 3; Methods).

67 A brief outline of previous determinations of the timing and duration of the LGM shows it  
68 extended from about 29.5 to 19 ka<sup>1</sup>. There is an initial rapid (>40 m) fall in GMSL from 31-32  
69 ka to 29-30 ka (Fig. 4a, 4b)<sup>1,2</sup>. A protracted gradual GMSL drop was construed from about 29  
70 ka to 21 ka<sup>2</sup>. However, this was largely an extrapolation between the two endpoints due to the  
71 sparsity of data which also have large (~20 m) uncertainties in RSL elevations (Fig 4c, 4e)<sup>2,5,6,7</sup>.  
72 Onset of deglaciation is apparent from 21 ka with a gradual 10-15 m GMSL rise<sup>2</sup> followed by a  
73 short stable or possibly slowly falling GMSL from ~18 ka to ~16.5 ka (see Figs. 4a, 4b of Ref.  
74 2). From here on, the deglaciation proceeded at a fast pace, at times, exceeding ~12 m/ky during  
75 the so-called meltwater pulses<sup>14,15</sup>.

76 We have converted our new GBR local sea levels to global values through GIA modelling  
77 (methods) which accounts for the higher GBR coastline elevations due to increased ice volumes  
78 and reduced adjacent ocean water loading. The present results significantly diverge from earlier  
79 determinations and completely revise the internal structure of the LGM GMSL (Fig. 4b). A

80 large number of data points from Noggin and Hydrographers sections show a relatively constant  
81 sea level from about 28 ka to 22 ka after the initial rapid fall from 31 ka<sup>2</sup> as documented  
82 previously from Barbados, Huon and Bonaparte Gulf (Figs. 3, 4c-4h). The GMSL remains  
83 invariant from 30 ka to 21.5 ka at mean value of 113 m within a range of about  $\pm 6$  m and  
84 represents the early LGM period, LGM-a (Fig. 4b; red band). This is significantly shallower  
85 than former estimates<sup>2</sup> (Fig. 4b). The previously identified<sup>16,17</sup>  $\sim 19$ ka, “onset-of-deglaciation”,  
86 in fact, corresponds to a rapid sea level fall followed by a  $\sim 4,000$  year-long  $\sim 3.5$  m/kyr sea level  
87 rise. We label this period as LGM-b, lasting from about 21 ka to 17 ka. The minimum GMSL at  
88 LGM-b ranges from about 130 m to 125 m due to analytical uncertainties and uncertainties in  
89 Earth model parameters and occurs after a  $\sim 20$  m drop (Methods, Extended Data Fig. 8,9 and  
90 Table 1). This point defines the start of LGM-b, after which the GMSL slowly rises to 120 m at  
91 about 17 ka followed by a rapid transition towards full deglaciation. The rate of net ice mass  
92 gain or sea-level fall at the inception of both the LGM-a ( $\sim 30$  ka) and LGM-b ( $\sim 21$  ka) are  
93 similar and range approximately from 15 to 20 mm per year as determined from the slopes of  
94 the GMSL curves. This GIA modelled, very fast, maximum glaciation rate is significantly  
95 faster than the mean LGM-Holocene deglaciation rate of  $\sim 12$  mm/year<sup>2</sup>. The sea-level drop at

96 LGM-b is strikingly evident in cores from both HYD and NOG sections as a major growth  
97 hiatus in cores M0031-33A and M0055A 33 (Fig. 2). Deposits of fresh water calcite cement, in  
98 corals below the hiatus, indicate subaerial exposure and low sea levels (Methods). In turn, the  
99 gap corresponding to the sea-level low is picked up at five other sites, M0035, 36, 39, 53 and  
100 54, at lower elevation, to complete the sea-level curve (Extended Data Fig. 3).

101 We have established an ice model, based on the new GBR RSL data that provides a good  
102 agreement with other far-field RSL records when combined with a range of Earth model  
103 parameters that span the possible range of viscosities for the upper and lower mantle as well as  
104 lithospheric thickness. Model predictions of RSL's, over the LGM-a and -b periods, generally  
105 agree well with the trends derived from existing data (Fig. 4, Extended Data Table 4). The  
106 magnitude of the sea level drop at the start of the LGM<sup>1,2</sup> ( $\approx 29$  ka) is about 40 m, constrained by  
107 coral data from Huon Peninsula<sup>18</sup> and Barbados<sup>19</sup> and with foraminifera oxygen isotope records  
108 from the Red Sea<sup>20</sup> within relatively large (ca.10 m) uncertainties. There is also close agreement  
109 between model results and data over the deglaciation period from 17 ka onwards except at  
110 Barbados (Fig. 4c). Here, the systematic overshoot of the data above the sea level curve is  
111 indicative of additional processes, possibly, of tectonic nature<sup>15</sup>. This is consistent with

112 independent evaluations including the study<sup>10</sup> using the rate of change of degree-two harmonics  
113 of Earth's geopotential due to GIA.

114 The very rapid build-up of global ice volume during the two periods of transition at LGM-a  
115 (~29-31 ka; Ref 2, Fig. 4D) and LGM-b (~22-21 ka; Fig. 4b, present work) requires substantial  
116 moisture transport and snow precipitation over existing ice sheets. To accommodate LGM-b an  
117 additional equivalent ice volume corresponding up to 17 m of sea level is required. The location  
118 of the extra ice cannot be determined with certainty. GIA modelling and Northern and Southern  
119 Hemisphere (NH, SH) bipolar climate paced by complementary high latitude insolation highs  
120 <sup>1,22</sup> at these times shows increased ice volume over the North American Ice Sheet (NAIS) at  
121 LGM whereas the Eurasian ice sheet appears to have grown at a slower pace and commenced  
122 melting after ≈22 ka (Extended Data Fig. 8). Colder Antarctic climate during the LGM<sup>4,16</sup> is  
123 likely to have hindered ice calving and lessened basal melting of ice shelves resulting in  
124 increased ice volume. The sustained growth of the AIS during the LGM-b period and beyond,  
125 including continuing ice accumulation up to around 14 ka, agrees with observations of the late  
126 retreat of West Antarctic Ice Sheet at this time <sup>1,23,24</sup>. However, the major increase in ice  
127 volume, precipitating the onset of LGM-b, appears to have been during a short period (20 ka to



128 21 ka) over the NAIS after which the NAIS retreated from  $\approx 20$  ka onwards<sup>25</sup> (Extended Data  
129 Fig. 8).

130 The enlarged global ice volume at  $\sim 30$  ka<sup>1,2,18,26</sup>, equivalent to  $\sim 40$  m of sea-level drop, persisted  
131 for over  $\sim 8$  thousand years. Similarly, the low NH insolation and somewhat reduced  
132 atmospheric CO<sub>2</sub> levels around  $\sim 21$  ka to  $\sim 22$  ka led to a period of cold climate, very low  
133 tropical Atlantic SST's and ultimately the transition to LGM-b. At this time, increased SH  
134 insolation is likely to have facilitated moisture transport to the South, increasing the AIS  
135 volume<sup>1,18,27</sup>. Heinrich event 1 at  $\sim 17$  ka marks the end of LGM-b when full deglaciation  
136 kicked-in as the pace of NH insolation and atmospheric CO<sub>2</sub> levels increased rapidly (Fig. 4).

137 The two sharp transitions preceding LGM-a and LGM-b periods, associated with rapid  
138 accumulation of ice and lower sea levels, at the end of the last ice age, do not appear to be  
139 explicable in terms of processes attributable to any specific climate-change dynamic. During  
140 this time ( $\sim 29$ - $19$  ka), oxygen isotope records in ice cores do not show a clear, distinct signal;  
141 the CO<sub>2</sub> levels were stable, insolation at the time was not so different to present and tropical  
142 SST did not change significantly<sup>1,28</sup>. A systematic behaviour in sea level and climate has  
143 previously been noted<sup>29</sup> whereby transitions between two states, cold to warm or warm to cold,

144 took place through a third more extreme state as in MIS3-LGM-Holocene or during the Last  
145 Interglacial (LIG), LIG-(LIG high-stand at the end of LIG)-(MIS 5d). A similar behaviour in  
146 climate was previously noted where the appearance of an intermediate, extreme third state, may  
147 have resulted in a shift from “41-ky” cycles to “100-ky” cycles 800 ka to 1 Ma ago<sup>30</sup>. These  
148 bifurcations can be thought of as states in three climate potentials with “stochastic climate  
149 noise” causing transitions between them<sup>30</sup>. Here, it appears that the same behaviour may occur  
150 over short timescales, not only over 100 ka cycles. The transitions are not only manifest in  
151 climate but are also associated with sea-level change.

152

### 153 **ACKNOWLEDGEMENTS**

154 We thank the IODP and ECORD (European Consortium for Ocean Research Drilling) for drilling the  
155 GBR, and the Bremen Core Repository for organizing the onshore sampling party. Financial support of  
156 this research was provided by the JSPS KAKENHI (JP26247085, JP15KK0151, JP16H06309,  
157 JP17H01168), Australian Research Council (grant DP1094001), ANZIC, NERC grant NE/H014136/1  
158 and Institut Polytechnique de Bordeaux.

159

160 **AUTHOR CONTRIBUTIONS**

161 Y.Y. and J.M.W. were co-chief scientists of Expedition 325. J.O. and Y.Y. conducted GIA modeling.

162 Y.Y. and T.M.E. wrote the manuscript in collaboration with J.M.W., A.L.T., J.C.B, M.H., and the paper

163 was refined by contributions from the rest of the co-authors.

164 **References:**

165 1. Clark, P. U., Dyke, A.S., Shakun, J.D., Carlson, A.E., Clark, J., Wohlfarth, B.,

166 Mitrovica, J.X., Hostetler, S.W., and McCabe, A.M. The Last Glacial Maximum. *Science* **325**,

167 710-714 (2009).

168 2. Lambeck, K., Rouby, H., Purcell, A., Sun, Y., Sambridge, M. Sea level and global

169 ice volumes from the Last Glacial Maximum to the Holocene. *Proceedings of National*

170 *Academy of Science of the United States of America* **111**, 15296-15303,

171 doi:10.1073/pnas.1411762111 (2014).

172 3. Felis, T., McGregor, H. V., Linsley, B. K., Tudhope, A. W., Gagan, M. K., Suzuki,

173 A., Inoue, M., Thomas, A. L., Esat, T. M., Thompson, W. G., Tiwari, M., Potts, D. C.,

174 Mudelsee, M., Yokoyama, Y., Webster, J. M.,. Intensification of the meridional temperature

- 175 gradient in the Great Barrier Reef following the Last Glacial Maximum. *Nature*  
176 *Communications* **5**, 4102, doi:10.1038/ncomms5102 (2014).
- 177 4. Mix, A. C., E. Bard, and R. Schneider. Environmental processes of the ice age: land,  
178 oceans, glaciers (EPILOG). *Quaternary Science Reviews* **20**, 627-657 (2001).
- 179 5. Yokoyama, Y., Lambeck, K., DeDeckker, P., Johnston, P., and Fifield, L.K. Timing  
180 of the Last Glacial Maximum from observed sea-level minima. *Nature* **406**, 713-716 (2000).
- 181 6. Fairbanks, R. G., A 17,000-year glacio-eustatic sea level record: influence of glacial  
182 melting dates on Younger Dryas event and deep ocean circulation. *Nature* **342**, 637-642 (1989).
- 183 7. Bard, E., B. Hamelin, and R.G. Fairbanks. U-Th ages obtained by mass spectrometry  
184 in corals from Barbados: sea level during the past 130,000 years. *Nature* **346**, 456-458 (1990).
- 185 8. Hanebuth, T., K. Stattegger, and P.M. Grootes. Rapid flooding of the Sunda Shelf: a  
186 late-glacial sea-level record. *Science* **288**, 1033-1035 (2000).
- 187 9. DeDeckker, P., and Y. Yokoyama. Micropalaeontological evidence for Late  
188 Quaternary sea-level changes in Bonaparte Gulf, Australia,. *Global and Planetary Change* **66**,  
189 85-92 (2009).

- 190 10. Nakada, M., Okuno, J., and Yokoyama, Y. Total meltwater volume since the Last  
191 Glacial Maximum and viscosity structure of Earth's mantle inferred from relative sea level  
192 changes at Barbados and Bonaparte Gulf and GIA-induced J2. *Geophysical Journal*  
193 *International* **204**, 1237-1253, doi:10.1093/gji/ggv520 (2016).
- 194 11. Weigelt, P., Steinbauer, M. J., Cabral, J. S. & Kreft, H. Late Quaternary climate  
195 change shapes island biodiversity. *Nature*, doi:10.1038/nature17443 (2016).
- 196 12. Webster, J. M., Braga, J.C., Humblet, M., Potts, D.C., Iryu, Y., Yokoyama, Y.,  
197 Fujita, K., Bourillot, R., Esat, T.M., Fallon, S., Thompson, W.G., Thomas, A.L., Kan, H.,  
198 McGregor, H.V., and Hinestrosa, G. Response of the Great Barrier Reef to sea level and  
199 environmental changes over the past 30 ka. *Nature Geoscience* **accepted** (2017).
- 200 13. Yokoyama, Y., and T.M. Esat. in *Handbook of Sea-Level Research* (ed I.  
201 Shennan, Long, A., and Horton, B.) Ch. 7, 104-124 (John Wiley & Sons, 2015).
- 202 14. Deschamps, P., N. Durand, E. Bard, B. Hamelin, G. Camoin, A.L. Thomas, G.M.  
203 Henderson, Okuno, J., and Y. Yokoyama. Ice-sheet collapse and sea-level rise at the Bølling  
204 warming 14,600 years ago. *Nature* **483**, 559-564 (2012).

- 205 15. Bard, E., B. Hamelin, and Delanghe-Sabatier, D. Deglacial Meltwater Pulse 1B and  
206 Younger Dryas Sea Levels Revisited with Boreholes at Tathiti. *Nature* **327**, 1235-1237 (2010).
- 207 16. Clark, P. U., A.M.McCabe, A.C.Mix, and A. J. Weaver. Rapid rise of sea level  
208 19,000 years ago and its global implications. *Science* **304**, 1141-1144 (2004).
- 209 17. MARGOProjectMembers. Constraints on the magnitude and patterns of ocean  
210 cooling at the Last Glacial Maximum. *Nature Geoscience* **2**, 127-132 (2009).
- 211 18. Cutler, K. B., R.L. Edwards, F.W. Taylor, H. Cheng, J. Adkins, C.D. Gallup, P. M.  
212 Cutler, G.S.Burr, and A.L. Bloom. Rapid sea-level fall and deep ocean temperature change  
213 since the last interglacial period. *Earth and Planetary Science Letters* **206**, 253-271 (2003).
- 214 19. Peltier, W. R., and Fairbanks, R.G. Global glacial ice volume and Last Glacial  
215 Maximum duration from an extended Barbados sea level record. *Quaternary Science Reviews*  
216 **25**, 3322-3337 (2006).
- 217 20. Grant, K. M., E. J. Rohling, M. Bar-Matthews, A. Ayalon, M. Medina-Elizalde, C.  
218 Bronk Ramsey, C. Satow and A.P. Roberts. Rapid coupling between ice volume and polar  
219 temperature over the past 150,000 years. *Nature* **491**, 744-747 (2012).

- 220 21. Abe-Ouchi, A. *et al.* Insolation-driven 100,000-year glacial cycles and hysteresis of  
221 ice-sheet volume. *Nature* **500**, 190-193, doi:10.1038/nature12374 (2013).
- 222 22. Pilippon, G., G. Ramstein, S. Charbit, M. Kageyama, C. Ritz, and C. Dumas.  
223 Evolution of Antarctic ice sheet throughout the last deglaciation: A study with a new coupled  
224 climate- north and south hemisphere ice sheet model. *Earth and Planetary Science Letters* **248**,  
225 750-758.
- 226 23. Anderson, J. B. *et al.* Ross Sea paleo-ice sheet drainage and deglacial history during  
227 and since the LGM. *Quaternary Science Reviews* **100**, 31-54,  
228 doi:10.1016/j.quascirev.2013.08.020 (2014).
- 229 24. Yokoyama, Y., Anderson, J.B., Yamane, M., Simkins, L.M., Miyairi, Y., Yamazaki,  
230 T., Koizumi, M., Suga, H., Kushara, K., Prothro, L., Hasumi, H., Southon, J.R., and Ohkouchi,  
231 N. Widespread collapse of the Ross Ice Shelf during the late Holocene. *Proceedings of National*  
232 *Academy of Science of United States of America* **113**, 2354-2359 (2016).
- 233 25. Lambeck, K., Purcell, A. & Zhao, S. The North American Late Wisconsin ice sheet  
234 and mantle viscosity from glacial rebound analyses. *Quaternary Science Reviews* **158**, 172-210,  
235 doi:10.1016/j.quascirev.2016.11.033 (2017).

- 236 26. Clark, P. U. & Tarasov, L. Closing the sea level budget at the Last Glacial  
237 Maximum. *Proc Natl Acad Sci U S A* **111**, 15861-15862, doi:10.1073/pnas.1418970111 (2014).
- 238 27. Clark, P. U., Hostetler, S.W., Pisias, N.G., Schmittner, A., and Meissner, K.J.  
239 Mechanisms for a ~7-kyr climate and sea-level oscillation during marine isotope stage 3. *Ocean*  
240 *Circulation: Mechanisms and Impacts* American Geophysical Union, Geophysical Monograph  
241 173, pp. 209-246. (2007).
- 242 28. Brook, E. J. *et al.* Timing of millennial-scale climate change at Siple Dome, West  
243 Antarctica, during the last glacial period. *Quaternary Science Reviews* **24**, 1333-1343,  
244 doi:10.1016/j.quascirev.2005.02.002 (2005).
- 245 29. Yokoyama, Y., and T.M. Esat. Global Climate and Sea Level-Enduring variability  
246 and rapid fluctuations over the past 150,000 years. *OCEANOGRAPHY* **24**, 54-69 (2011).
- 247 30. Paillard, D. Quaternary glaciations: from observations to theories. *Quaternary*  
248 *Science Reviews* **107**, 11-24, doi:10.1016/j.quascirev.2014.10.002 (2015).
- 249
- 250 **Methods**
- 251 **IODP Expedition 325: The Great Barrier Reef environmental changes.**



252 The Integrated Ocean Drilling Program (IODP) Expedition 325 was designed to complement  
253 the previous IODP “Tahiti Sea Level” Expedition 310 to Tahiti<sup>31</sup>. In preparation for Expedition  
254 325, potential drill sites were surveyed with the CSIRO ship *RV Southern Surveyor* using  
255 multibeam sonar, seismics, an AUV and rock dredging<sup>12,32</sup>. At most of the Great Barrier Reef  
256 (GBR) locations, the shelf breaks at approximately 120 m and is populated with prominent  
257 terrace-like structures and other relict reefs appear successively at 100-90 m, 60-50 m and 35-40  
258 m depths<sup>33-35</sup>.

259 The mission specific platform chosen for Expedition 325 was the *Greatship Maya*, an IMO  
260 class II vessel capable of being positioned dynamically for *geotechnical* coring<sup>32,35</sup>. The  
261 expedition took place between 12 February and 6 April 2010. A total of 34 holes across 17 sites  
262 were sampled ranging in depth from 46.4 m to 170.3 m such that the recovered coralgal deposits  
263 span several crucial but poorly defined periods during the LGM and last deglaciation. Sampling  
264 occurred at three locations along the North Eastern coast of Australia but this study focuses on  
265 one transect at 19.7° latitude offshore from Cairns at Noggin Pass (NOG-01B), and another at  
266 17.1° latitude, offshore Mackay at Hydrographer’s Passage (Fig. 1, HYD-01C). Photographs of  
267 half-sectioned reef cores, relevant to the present study, are shown in (Extended Data, Figs. 1, 2)

268 together with the depths and genera of the dated corals and coralline algae. Classification of  
269 coral genera and species in terms of their habitat preferences according to depth and turbulence  
270 levels is also supported by considering the habitats of associated coralline algae taxa and crust  
271 thickness and vermetid gastropods. For example, individual coralline algae can have limited  
272 range of habitats bounded by sensitivity to light levels, wave energy and other factors and can  
273 be used to more accurately constrain the paleo-depth ranges. Based on this careful and detailed  
274 multi-proxy approach each dated coral and coralline algae sample was placed within an  
275 internally consistent coralgal assemblage and paleobathymetric scheme<sup>36,37</sup> enabling the  
276 construction of an independent RSL envelope at each site (Extended Data Figs. 1, 2, 3, Table 1  
277 and 2).

278

279 **Main lithologic facies observed in the Expedition 325 cores.**

280 The main lithologies are divided into coral reef framework and detrital sedimentary facies. The  
281 three boundstone facies are defined by their varying proportions of corals, coralline algae and  
282 microbial deposits forming coralgal, coralgal-microbialite and microbialite-dominated  
283 boundstones. The detrital facies can occur locally as internal sediments within the boundstones,

284 or as metre scale intervals of packstones to rudstones and unconsolidated sediments. Details of  
285 facies and depth estimate using facies as well as coral and coralline algae assembly can be  
286 found in Extended Data Figures 1 and 2 and Table 1, and are derived from Webster et al.<sup>12</sup>.

287

### 288 **Reef 2 hiatus and GMSL drop to LGM-b**

289 A major growth hiatus is observed in the inner shelf terrace at 104-106 mbsl, at both HYD-01C  
290 M0031-33A) and NOG-01B (Hole M0055A) (Extended Data Figs. 3 and 4)<sup>12</sup>. This represents  
291 the turn-off of Reef 2 at ~ 21 ka and is interpreted to be caused by the drop in sea-level to the  
292 LGM-b. The coralgial assemblages show that paleowater depths were shallow (<10 m) just prior  
293 to Reef 2 death, and lithologic, and seismic evidence indicates this was a major subaerial  
294 exposure surface<sup>12</sup>. Furthermore, detailed scanning electron microscopic (SEM),  
295 energy-dispersive X-ray spectrum (SEM-EDS), X-ray diffraction (XRD) analyses and  
296 thin-section observations of Reef 2 deposits confirm that they were exposed to freshwater or  
297 subaerial environments (e.g. low magnesium calcite cements in Hole 55A Core 4R1) during the  
298 sea level lowstand at LGM-b (Extended Data Fig 5). At this time shallow reef development  
299 migrated ~3 to 0.4 km seaward (ie. Reef 3a) in <2 kyr, as the RSL sea level fell to 118 m below

300 present by ~20.5 ka. The Reef 3a deposits and the older > MIS3 deposits are characterized by  
301 wholly marine diagenetic features consistent with the interpretation that the LGM-b sea level  
302 did not fall below this level (Extended Data Fig 6). Sea level rose during the deglacial causing  
303 major Reef 3a aggradation<sup>12</sup> before re-flooding the inner shelf terraces at ~ 16.5 ka and causing  
304 the re-establishment of the reef (Reef 3b) over its former position, marking the end of the hiatus  
305 at the top of Reef 2.

306

### 307 **Determining the ages of sea level indicators**

308 Representative, more than 165, coral skeletons and their aragonite content were analyzed by  
309 powder X-ray diffraction, X-radiography, SEM and petrologic investigations, all of which  
310 confirmed to the pristine nature of the dated samples<sup>3</sup>. In a few cases, X-ray diffraction picked  
311 up minor signatures of Hi-Mg calcite, likely due to trace amounts of coralline algae and  
312 microbialite sediment. Yet no significant calcite peaks were observed in most of the cases.  
313 Physical cleaning of branched corals for U-Th dating and severe acid dissolution of samples,  
314 namely more than 50% of the weight, for radiocarbon dating was used to remove potential  
315 secondary precipitated materials. For massive *Porites* corals, physical cleaning is difficult

316 requiring further geochemical tests including ICP-MS. Skeletal Mg/Ca ratios confirmed the  
317 absence of significant amounts of high-Mg calcite and secondary aragonite cements. Even the  
318 case when the secondary aragonite was found, the ages are not affected significantly since the  
319 form of the cements are indicative of early phase of post mortem of corals. Further evaluations  
320 included limits on total uranium,  $^{232}\text{Th}$  content and initial  $^{234}\text{U}/^{238}\text{U}$  ratio. We applied different  
321 initial  $^{234}\text{U}/^{238}\text{U}$  criteria: for samples of the deglacial period between 17 ka and 0 ka, the  
322 acceptable range was 1.1452 +/- 0.0140, whereas for the samples from 30 ka to 17 ka 1.1402  
323 +/-0.0140 was used. All of data used to reconstruct the relative sea level envelopes for each  
324 transect are shown in Extended Data Tables 2 and 3 (see Methods Section *Relative Sea level*  
325 *(RSL) reconstruction* for more details) and the primary samples used to determine the specific  
326 RSL inflection points are indicated as “HY-1, 2..” and “NO-1, 2..” for HYD-01C and NOG-01B  
327 respectively in the Extended Data Table 2 and highlighted in bold. U-series and radiocarbon  
328 ages from the same coral samples also showed remarkable consistency, along with radiocarbon  
329 ages on directly adjacent coralline algae. Taken together, and combined with the consistent  
330 reproducibility of the relative sea level envelopes between two transects, more than 500 km  
331 apart, confirms the veracity of the data.

332

333 **Radiocarbon dating**

334 More than 500 radiocarbon dates were obtained using corals and coralline algae samples which  
335 were all processed at the Atmosphere and Ocean Research Institute (AORI), the University of  
336 Tokyo (UTokyo) to convert them into graphite<sup>38</sup>. Typically 1mg or more of graphite was  
337 measured using a Single Stage Accelerator Mass Spectrometry at AORI<sup>39</sup> and at the Australian  
338 National University (ANU; <sup>40</sup>). The results were then converted to calendar ages with local  
339 reservoir ages ( $12\pm 10$  years) from<sup>41</sup>, which we obtained by averaging between Heron Island  
340 ( $8\pm 6$  years) and Abraham Reef values ( $15\pm 6$  years). The calibration was then performed using  
341 international calibration datasets (IntCal 13 and Marine 13;<sup>42</sup>)

342

343 **Analytical procedures, Mass spectrometry and U-Th dating.**

344 The analytical data are listed in Extended Data Table 3. Consistency between labs for replicate  
345 measurements of a single specimen is within 100 years, which is similar to the intra coral  
346 variability observed in some specimens measured using the high precision (WHOI) method.

347 Uranium series dating were conducted at three different labs: the Australian National University  
348 (ANU), the University of Oxford (OX) and the Woods Hole Oceanographic Institute (WHOI).  
349 A 61-cm mass spectrometer is used at ANU, which can operate in charge-mode<sup>43</sup>. The  
350 <sup>229-230-232</sup>Th isotopes were measured simultaneously in charge-mode in Faraday cups using 20pF  
351 feed-back capacitors as active electrometer elements. Uranium isotopes, <sup>233-234-235</sup>U were also  
352 measured in charge-mode, whereas <sup>238</sup>U was simultaneously measured using a 10<sup>10</sup> Ohm  
353 feed-back resistor. The magnitude of the <sup>238</sup>U low-mass tail was monitored continuously at mass  
354 <sup>237</sup>U in charge mode. This was used to subtract the <sup>238</sup>U tail from under the <sup>233-234-235</sup>U isotopes.  
355 Extensive measurements with an un-spiked U-standard HU-1 showed that the shape of the <sup>238</sup>U  
356 tail remained invariant under a wide range of conditions, in particular, at the expected locations  
357 of the <sup>233-236</sup>U peaks. Sample loads, on single rhenium filaments, ranged from 0.5 to 0.8 µg and  
358 the <sup>238</sup>U beam intensity was kept between 8x10<sup>11</sup> to 10x10<sup>11</sup> Ampere for several hours. At these  
359 intensities, 10<sup>10</sup> Ohm feedback resistor was used to avoid response-time problems encountered  
360 with the considerably slower 10<sup>11</sup> Ohm resistors. The instrument was calibrated with reference  
361 to a secular-equilibrium standard HU-1. Comparisons with Western Australian last interglacial  
362 samples<sup>44</sup> and with Hulu-Cave speleothem data<sup>45</sup> showed precise agreement with previous

363 measurements. Sample processing followed previously established procedures<sup>46</sup>. U and Th were  
364 separated from the coral carbonate using U-Teva resin in a single pass.

365

366 Uranium thorium dating at OX and WHOI were measured by multi-collectors ICP-MS. At OX,

367 U and Th isotopes were measured with ion counter collectors for the minor isotope beams.

368 Approximately 0.3g of coral sample was dissolved and spiked with a mixed <sup>236</sup>U:<sup>229</sup>Th tracer. U

369 and Th were purified and measured separately: U isotopes, statically; and Th by peak hopping

370 the 229 and 230 beams into an ion counter while normalizing beam intensity between the steps

371 with either <sup>232</sup>Th or <sup>235</sup>U measured in Faraday collectors. Instrumental biases and relative

372 collector efficiencies are accounted for using standard sample bracketing using U and Th

373 isotope standards<sup>47</sup>.

374

375 At WHOI U and Th isotopes were measured by MC-ICP-MS in static mode with all isotopes in

376 Faraday collectors<sup>48</sup>. Large ~5g subsamples of coral were dissolved and spiked with a mixed

377 <sup>233</sup>U:<sup>236</sup>U:<sup>229</sup>Th tracer, optimised for the last glacial maximum to deglacial age samples, and



378 co-precipitated with Fe. To determine the  $^{230}\text{Th}/^{238}\text{U}$ , purified U and Th fractions are  
379 recombined such that U and Th are measured together at isotope ratios that can be closely  
380 matched to bracketing standards. The  $^{234}\text{U}/^{238}\text{U}$  is similarly determined statistically in Faraday  
381 collectors but on an unspiked aliquot.

382

383 All activity ratios and ages are calculated using the half-lives reported in<sup>45</sup>. Ages are presented  
384 in Extended Data Table 1 as 'raw', assuming all  $^{230}\text{Th}$  is accumulated in the coral since growth,  
385 and an age corrected for detrital  $^{230}\text{Th}$ . The detrital correction makes use of the measured  
386  $^{232}\text{Th}/^{238}\text{U}$  as a proxy for the amount of detrital contamination, an assumed detrital composition  
387 of crustal origin<sup>49</sup>, and an allowance for non-secular equilibrium of the contaminant.

388

### 389 **Relative sea level (RSL) reconstruction**

390 The sample context was assessed using established criteria<sup>12,32</sup> including: (1) core quality, (2)  
391 orientation of well-preserved corallites; (3) thick coralline algal crusts capping upper coral  
392 surfaces; (4) evidence of substrate attachment; and (5) the presence/absence and orientation of

393   geopetals in lithified facies . Based on these criteria all the samples were classified into the  
394   following four context categories: (1) IS = in situ (convincing supporting evidence), (2) IS? =  
395   likely insitu (inclusive supporting evidence), (3) ISX = not in situ (convincing nonsupporting  
396   evidence, and (4) ISN = status not known (inadequate evidence either way). Samples from  
397   highly drill-disturbed or poor recovery intervals were excluded. A total of 540 samples  
398   satisfying these criteria were used to construct a RSL envelope (upper and lower bounds) at  
399   both sites. Despite known temporal differences in ocean reservoir age, the coral U/Th and  
400   coral/coralline <sup>14</sup>C AMS ages are remarkably consistent. However, wherever possible we used  
401   the more precise U/Th coral ages to constrain the upper and lower bounds of the envelopes. This  
402   was achieved by visually fitting a line through the dates that were >1 m apart and outside their  
403   analytical age errors, while also taking into account the upper bound of the paleowater depth  
404   estimate of each sample and any core recovery uncertainties (Extended Data Table 2). Where  
405   multiple coral dates overlapped (in time) we used the mid-point between samples. If replicate  
406   age determinations were available for the same sample (ie. same coral colony or coralline algal  
407   crust) (Extended Data Table 2) an average age was calculated and plotted on Fig. 3. The upper  
408   bound or minimum position of the sea level envelope was further constrained by considering the

409 overlapping paleowater depth ranges of both the shallow water sea level indicators and their  
410 coeval, deeper forereef slope equivalents. Finally, the major inflection points marking clear  
411 changes in the direction, amplitude and rate of RSL change were also identified each envelope  
412 (Fig. 3). Thus the lower bound (i.e. maximum sea level position) of RSL curves and the specific  
413 samples defining them are indicated in bold in Extended Data Table 2 (ie. HY-1, 2., NO-1, 2.)  
414 and a close up of the key samples constraining LGM-b is also shown in Extended Data Figure 6.

415

416

#### 417 **GIA model predictions**

418 The GIA model calculations included an earth model describing the viscoelastic properties of  
419 the solid earth, as well as an ice component documenting the ice melting history, reconstructed  
420 mainly from far-field sea-level observations<sup>2,50</sup>. The Earth model is based on seismologically  
421 derived “Preliminary Reference Earth Model” (PREM)<sup>51</sup> and consisted of an elastic lithosphere  
422 with an upper and lower mantle divide at 670 km depth. The lithosphere thickness was 70km  
423 and upper and lower mantle viscosities ranged from  $(1-10) \times 10^{20}$  Pas and  $(1-100) \times 10^{22}$  Pas

424 respectively. This model provides an accurate treatment of time-dependent continental  
425 shorelines<sup>52</sup> and the Earth rotation feedback on sea level<sup>53</sup>.

426 The ice model described above was adjusted to match the newly obtained (RSL) records from  
427 the Great Barrier Reef. The analytical uncertainties in RSL were taken into account and the  
428 shallow and deep extremes of the RSL envelope were tested. We first employed the ice history  
429 model developed by ANU group<sup>2</sup> and ran the GIA model to obtain relative sea level histories  
430 for the GBR. The ANU ice model with the same relative ice volumes was then scaled to fit the  
431 NOG and HYD RSL. The scaling was done manually within a reasonable range of various  
432 parameters and by keeping the relative ice volume of various ice sheets the same as in the  
433 original ANU model though keeping the Eurasian ice model almost the same as the ANU model  
434 since the history of this ice sheet is reasonably well constrained from both observations and  
435 models<sup>54-56</sup> compared to other ice sheets. The chosen Earth parameters (Lithospheric thickness =  
436 70km, Upper mantle viscosity =  $2 \times 10^{20}$  Pa s, and Lower mantle viscosity =  $10^{22}$  Pa s)<sup>57,58</sup> fit  
437 the GBR region Holocene sea levels well. The analytical uncertainties in RSL and the range in  
438 Earth Model parameters (approximately  $\pm 2.5$  m contribution to GMSL) were used in calculating  
439 the MAX and MIN extremes (Extended Data Figs. 8, 9 and Table 4). Extended Data Table 2

440 shows Global Mean sea level contributions individually for each major ice sheet and for the  
441 ANU and highest SL and lowest SL GMSL scenarios (in eustatic terms). The two GMSL curves  
442 were then used to construct RSLs in far-field sites with previously published RSL data for  
443 comparison (Fig. 4 and Extended Data Fig. 7). Potential Earth model uncertainties were also  
444 considered with variable lithosphere thickness and a range of viscosities, of the lower as well as  
445 the upper mantle, resulting in more than 60 GIA model experiments. Shaded areas of curves  
446 represent possible ranges in RSL for individual sites (Fig. 4 and Extended Data Fig. 7). Visual  
447 inspection of the results indicate that the MAX model fits the data remarkably well for almost  
448 all the far-field locations tested. In turn, this indicates that the shallow coral habitat depth  
449 estimates appear to be sufficiently robust without necessitating extended, deeper water limits.

450 During the last glacial maximum (30-19 ka; Fig. 3), water depth uncertainties for most samples  
451 from the HYD and NOG transects are <5m. Figure 2 shows RSL curves derived from MAX and  
452 MIN models. Various Earth rheology parameters were also tested using both MAX and MIN ice  
453 models where the shaded region around GMSLs in Extended Data Figure 9 represents the  
454 corresponding range in RSLs. During the LGM, the maximum magnitude of RSL difference  
455 between the two transects is less than 10 m<sup>59</sup> and hence RSL variations arising from

456 hydro-isostasy are small. The models were run over the maximum possible ranges of the  
457 rheological parameters so that the range of RSLs depicted as the shaded zone in Extended Data  
458 Fig. 9 cover the full range of possibilities. Traditionally, lower mantle viscosity has been  
459 estimated as ca.  $10^{22}$  Pa s using far-field RSL observations<sup>57,58</sup>, whereas recent studies have  
460 reported much higher values of  $\sim 7 \times 10^{22}$  Pa s<sup>3</sup>. Thus, assuming a typical lithospheric thickness  
461 and upper mantle viscosity respectively of 70km and  $2 \times 10^{20}$  Pa s, the maximum RSL  
462 differences associated with the above range of lower mantle viscosities is ca. 5m (Extended  
463 Data Figure 9). This number is smaller than the typical uncertainties inherent in RSL  
464 observations at the GBR and, therefore, is well suited for reconstructions of GMSLs during  
465 LGM-a and LGM-b. In summary, we concluded that the MAX model provides the best estimate  
466 of GMSLs as well as indicating that these tighter depth uncertainties for GBR corals<sup>12</sup> do  
467 provide consistent results. Therefore, the extended MIN to MAX range, employed here, well  
468 covers the likely range of GMSL constructions with confidence as can be ascertained by visual  
469 inspection (Extended Data Figure 9).

470 Glaciological evidence, including from ice cores cannot easily accommodate the required  
471 increase in ice volume. However, the total increase is shared among the large ice sheets

472 (Extended Data Fig. 8). Ice cores retrieved from Antarctica and Greenland are not able to  
473 resolve the required magnitude of elevation changes in continental interiors. It is also likely that  
474 current ice free regions may have been the places to retain the extra ice at these times. For  
475 example, recent evidence suggests that an extensive Ice sheet was grounded on the Ross Sea for  
476 at least 3,700 years<sup>60</sup>. New bathymetric data as well as glacial models support these  
477 conclusion<sup>61</sup>. However, there is still scope to improve the glaciological models and hence, we  
478 hope that our data will contribute to this effort.

479 Discrepant GMSLs during the LGM at either -120 m or -140 m has been reported respectively  
480 for Barbados<sup>7</sup> and the Bonaparte Gulf in North Australia<sup>5</sup>. This has now been reconciled using  
481 the recently reported Earth rheology model with J2 observations<sup>10</sup> as well as considering  
482 subducting material in Barbados<sup>62</sup>. The model included 65-100km of lithospheric thickness and  
483 upper and lower mantle viscosities of  $(1-3) \times 10^{20}$  Pa s and  $10^{23}$  Pa s. The global relative sea  
484 level observations could reasonably be explained if GMSL during the LGM was ca. -130m.  
485 This finding is consistent with the model derived from more than 1,000 far-field RSL  
486 observations<sup>2</sup>. The results from the present study, for both the MAX and the MIN options, are

487 respectively -125m and -130m and thus consistent with the independent estimates described  
488 above.

489

490

491 31. Camoin, G. F., Seard, C., Deschamps, P., Webster, J.M., Abbey, E., Braga, J.C.,  
492 Iryu, Y., Durand, N., Bard, E., Hamelin, B., Yokoyama, Y., Thomas, A.L., Henderson, G.M.,  
493 and Dussouillez, P. Reef response to sea-level and environmental changes during the last  
494 deglaciation. IODP Expedition 310 "Tahiti Sea Level". *Geology* **40**, 643-646 (2012).

495 32. Webster, J. M., Yokoyama, Y., Cotterill, C., and Expedition325Scientist.  
496 *Proceedings of the Integrated Ocean Drilling Program 325; Expedition Reports Great Barrier*  
497 *Reef Environmental Changes.* (Integrated Ocean Drilling Program Management International,  
498 Inc., 2011).

499 33. Abbey, E., Webster, J. M., and Beaman, R. J. . Geomorphology of submerged reefs  
500 on the shelf edge of the Great Barrier Reef: The influence of oscillating Pleistocene sea-levels. .  
501 *Marine Geology* **288**, 61-78 (2011).



- 502 34. Bridge, T. C. L., Done, T.J., Beaman, R.J., Friedman, A., Williams, S.B., Pizarro, O.,  
503 and Webster, J.M. Topography, substratum and benthic macrofaunal relationships on a tropical  
504 mesophotic shelf margin, central Great Barrier Reef, Australia. *Coral Reefs* **30**, 143-153 (2011).
- 505 35. Yokoyama, Y., Webster, J.M., Cotterill, C., Braga, J.C., Jovane, L., Mills, H.,  
506 Morgan, S., Suzuki, A. and the IODP 325 Scientists IODP Expedition 325: The Great Barrier  
507 Reef Reveals Past Sea-Level, Climate and Environmental Changes since the Last Ice Age.  
508 *Scientific Drilling* **12**, 32-45 (2011).
- 509 36. Cabioch, G., Montaggioni, L.F., Faure, G., Ribaud-Laurenti, A. Reef coralgal  
510 assemblages as recorders of paleobathymetry and sea-level changes in the Indo-Pacific  
511 province. *Quaternary Science Reviews* **18** (14), 1681–1695 (1999).
- 512 37. Dechnik, B., Webster, J.M., Webb, G.E., Nothdurft, L., Dutton, A., Braga, J.-C.,  
513 Zhao, J.-X., Duce, S. and Sadler, J. The evolution of the Great Barrier Reef during the Last  
514 Interglacial Period. *Global and Planetary Change* **149**, 53–71 (2017).
- 515 38. Yokoyama, Y., Miyairi, H., Matsuzaki, F. and Tsunomori. Relation between acid  
516 dissolution time in the vacuum test tube and time required for graphitization for AMS target

517 preparation, . *Nuclear Instruments and Methods in Physics Research Section B* **259**, 330-334  
518 (2007).

519 39. Hirabayashi, S., Yokoyama, Y., Suzuki, A., Miyairi, Y. & Aze, T. Multidecadal  
520 oceanographic changes in the western Pacific detected through high-resolution bomb-derived  
521 radiocarbon measurements on corals. *Geochemistry, Geophysics, Geosystems* **18**, 1608-1617,  
522 doi:10.1002/2017gc006854 (2017).

523 40. Fallon, S. J., Fifield, L. K. & Chappell, J. M. The next chapter in radiocarbon dating  
524 at the Australian National University: Status report on the single stage AMS. *Nuclear  
525 Instruments and Methods in Physics Research Section B: Beam Interactions with Materials and  
526 Atoms* **268**, 898-901, doi:10.1016/j.nimb.2009.10.059 (2010).

527 41. Druffel, E. R. M. & Griffin, S. Variability of surface ocean radiocarbon and stable  
528 isotopes in the southwestern Pacific. *Journal of Geophysical Research: Oceans* **104**,  
529 23607-23613, doi:10.1029/1999jc900212 (1999).

530 42. Reimer, P. J., Bard, E., Bayliss, A., Beck, J.W., Blackwell, P.G., Bronk Ramsey, C.,  
531 Buck, C.E., Cheng, H., Edwards, R.L., Friedrich, M., Grootes, P.M., Guilderson, T.P.,  
532 Hafliðason, H., Hajdas, I., Hatté, C., Heaton, T.J., Hoffmann, D.L., Hogg, A.G., Hughen, K.A.,

533 Kaiser, K.F., Kromer, B., Manning, S.W., Niu, M., Reimer, R.W., Richards, D.A., Scott, E.M.,  
534 Southon, J.R., Staff, R.A., Turney, C.S.M., and van der Plicht, J. INTCAL13 and Marine13  
535 radiocarbon age calibration curves 0-50,000 years cal BP. *Radiocarbon* **55**, 1869-1887 (2013).

536 43. Esat, T. M. Charge collection thermal ion mass spectrometry of thorium.  
537 *International Journal of Mass Spectrometry and Ion Processes* **148**, 159-171 (1995).

538 44. Stirling, C. H., Esat, T. M., Lambeck, K., and McCulloch, M. T. . Timing and  
539 duration of the last interglacial; evidence for a restricted interval of widespread coral reef  
540 growth. . *Earth and Planetary Science Letters* **160** (1998).

541 45. Cheng, H., Edwards, R.L., Hoff, J., Gallup, C.D., Richards, D.A., and Asmerom, Y.  
542 The half-lives of uranium-234 and thrium-230. *Chemical Geology* **169**, 17-33 (2000).

543 46. Stirling, C. H., Esat, T.M., McCulloch, M.T., and Lambeck, K. High-precision  
544 U-series dating of corals from Western Australia and implications for the timing and duration of  
545 the Last Interglacial *Earth and Planetary Science Letters* **135**, 115-130 (1995).

546 47. Thomas, A. L., G. Henderson, P. Deschamps, Y. Yokoyama, A.J. Mason, E. Bard, B.  
547 Hamelin, N. Durand, and G. Camoin. Penultimate Deglacial Sea Level Timing from  
548 Uranium/Thorium Dating of Tahitian Corals. *Science* **324**, 1186-1189 (2009).

- 549 48. O’Leary, M. J. *et al.* Ice sheet collapse following a prolonged period of stable sea  
550 level during the last interglacial. *Nature Geoscience* **6**, 796-800, doi:10.1038/ngeo1890 (2013).
- 551 49. Taylor, S. R., and McLennan, S.M. *The continental crust: Its composition and*  
552 *evolution : An examination of the geochemical record preserved in sedimentary rocks.* .  
553 (Blackwell Scientific, 1985).
- 554 50. Okuno, J., Nakada, M., Ishii, M., and Miura, H. Vertical tectonic crustal movements  
555 along the Japanese coastlines inferred from late Quaternary and recent relative sea-level  
556 changes. *Quaternary Science Reviews* **91**, 42-61 (2014).
- 557 51. Dziewonski, A. M., and Anderson, D.L. Preliminary reference Earth model (PREM).  
558 *Physics of the Earth and Planetary Interiors* **25**, 297-356 (1981).
- 559 52. Lambeck, K., A. Purcell, P. Johnston, M. Nakada, and Y. Yokoyama. Water-load  
560 definition in the glacio-hydro-isostatic sea-level equation. *Quaternary Science Reviews* **22**,  
561 309-318 (2003).
- 562 53. Boulton, G. S., P. Dongelmans, M. Punkari, and M. Broadgate. Palaeoglaciology of an  
563 ice sheet through a glacial cycle: the European ice sheet through the Weichselian. *Quaternary*  
564 *Science Reviews* **20**, 591-625 (2001).

- 565 54. Lambeck, K., C. Smither, and P. Johnston. Sea-level change, glacial rebound and  
566 mantle viscosity for northern Europe. *Geophysical Journal International* **134**, 102-144 (1998).
- 567 55. Lambeck K, A. Purcell, J. Zhao, N.-O. Svensson. The Scandinavian Ice Sheet: From  
568 MIS 4 to the end of the Last Glacial Maximum. *Boreas* **39**, 410–435 (2010). □
- 569 56. Milne, G. A., and Mitrovica, J.X. Post glacial sea-level change on a rotating earth.  
570 *Geophysical Journal International* **133**, 1-19 (1998).
- 571 57. Nakada, M., and Lambeck, K. Late Pleistocene and Holocene sea-level change in the  
572 Australian region and mantle rheology. *Geophysical Journal* **96**, 497-517 (1989).
- 573 58. Lambeck, K., and Nakada, M. Late Pleistocene and Holocene sea-level change along  
574 the Australian coast. *Global and Planetary Change* **89**, 143-176 (1990).
- 575 59. Yokoyama, Y., A. Purcell, J.F.Marshall, and K. Lambeck. Sea-level during the early  
576 deglaciation period in the Great Barrier Reef, Australia. *Global and Planetary Change*, **53**,  
577 147-153, (2006).

578 60. Bart, P., B.J.Krogmeier, M.P.Bart, and S.Tulaczyk. The paradox of a long grounding  
579 during West Antarctic Ice Sheet retreat in Ross Sea. *Scientific Reports*, **7**, 1262,  
580 doi:10.1038/s41598-017-01329-8, (2017).

581 61. Halberstadt, A. R. W., Simkins, L. M., Greenwood, S. L. & Anderson, J. B. Past  
582 ice-sheet behaviour: retreat scenarios and changing controls in the Ross Sea Antarctica. *e*  
583 *Cryosphere* **10**(3), 1003–1020, doi:10.5194/tc-10-1003-2016 (2016).

584 62. Austermann, J., J.X.Mitrovica, K.Latychev, and G.A.Milne. Barbados-based  
585 estimate of ice volume at Last Glacial Maximum affected by subducted plate. *Nature*  
586 *Geoscience*, **6**, 553-557. doi:10.1038/NGEO1859.

587 63. Edwards, R.L., J.W. Beck, G.S. Burr, D. J. Donahue, J.M.A. Chappell, A. L. Bloom,  
588 E.R.M. Druffel, and F.W. Taylor. A large drop in atmospheric  $^{14}\text{C}/^{12}\text{C}$  and reduced melting in  
589 the Younger Dryas, documented with  $^{230}\text{Th}$  ages of corals. *Science*, **260**, 962-968 (1993).

590

## 591 **Figure Captions**

592 **Figure 1 | Location of GBR Expedition 325 study site at Cairns (Noggin Pass - NOG-01B)**

593 **and at Mackay (Hydrographer's Passage – HYD-01C).** High-resolution 3D multibeam

594 image showing the surface geomorphic context<sup>12</sup>, drill transects and specific locations of the  
595 drill holes.

596 **Figure 2 | Last Glacial Maximum sea level drop LGM-b captured clearly as a distinct age**  
597 **discontinuity observed in cores M0055A and M0031-33A from NOG and HYD transects**  
598 **respectively, separated by more than 500 km in the GBR** (Extended Data Table 1, Figs. 1,  
599 2). Cores obtained from different fossil GBR terraces and reefs reveal the trajectory of past sea  
600 level changes. Five reef sequences are distinguished based on the IODP Exp. 325 record: Reef 1  
601 ( $\geq 30$  ka), Reef 2 (27-22 ka), Reef 3 (3a, 21-17 ka; 3b, 17-13 ka), Reef 4 (13-10 ka), and Reef 5  
602 (modern GBR). The major growth hiatus evident from both HYD and NOG sections marks the  
603 death of Reef 2 (22.1 ka to 21.9 ka) following the sea level fall leading to LGM-b and  
604 reestablishment of reef (Reef 3a) further seaward at 20.7-20.5 ka (Extended Data Figs. 3, 4, 5).  
605 The age versus depth relationships, and the presence of fresh water low magnesium calcite  
606 cement, in Reef 2, confirms subaerial exposure during the LGM-b period. In contrast, their  
607 absence below Reef 3a deposits places a maximum limit on the sea level fall (Methods). At the  
608 end of LGM, after 17 ka, sea level rose rapidly flooding the outer shelf causing the  
609 re-establishment of the reef over its former position (Reef 3b), marking the end of hiatus at the

610 top of Reef 2 at ~17 ka. The details of the transition to LGM-b and the critical samples defining  
611 the fall in sea-level are shown in Extended Data Fig. 6.

612 **Figure 3 | Age versus depth plots showing the RSL envelopes at Cairns (red) and Mackay**

613 **(blue) derived from samples recovered by IODP Exp 325.** Both NOG and HYD transect

614 cores were examined for coral, coralgal algae and benthic foraminiferal assemblages (Extended

615 Data Figs. 1, 2) with help of X-ray CT scan and X-ray diffraction (Extended Data Table 1, 2)

616 that revealed detailed features of relative sea level histories during the past 35,000 years. The

617 >500 dates, selected through detailed sedimentologic and biologic analyses (Methods), provided

618 a robust chronostratigraphic framework that defined five distinct reef sequences (Reefs 2 to 4

619 are labeled on Fig. 2) which grew episodically over the past 30 ka. The RSL's constructed here

620 depend on the age (horizontal grey line) and sea level depth uncertainties (upward and

621 downward grey lines) related to paleo-habitat depth range (upward line) of each dated coral or

622 algal sample and the maximum coring depth uncertainty (downward line). The paleowater

623 depths were conservatively estimated using a multiproxy approach combining coral, coralline

624 algae and other key indicators such as algal crust thickness, and the presence of vermetid

625 gastropods (Methods, Extended Table 1). Note the disconnected paleowater depth lines on some



626 samples are indicative of deeper habitat ranges likely > 20 m water depth. The distribution of  
627 marine and fresh water cements in the cores were used to support the new estimates of the  
628 timing and magnitude of the LGM-b sea levels (Extended Data Figs. 3-5), including hiatuses  
629 and regressions.

630 **Figure 4 | Global mean sea levels over the past 140 ka (a, b) and GIA model predictions of**  
631 **relative sea levels for various far-field locations (c-h).** Previously constructed mean sea level  
632 curve, blue line<sup>2</sup> in panels a and b, is shown together with the inferred GMSL using GBR RSL  
633 data (orange band); High latitude (65 °) summer insolation curves for Northern and Southern  
634 Hemispheres in panel (b) are shown as dashed orange and blue lines respectively. Long term sea  
635 level variation is in step with Northern Hemisphere summer insolation whereas LGM-b occurs  
636 at the peak of Southern Hemisphere insolation. Results of 62 GIA model runs (Methods), over a  
637 range of potential earth model parameters, such as lithospheric thickness and viscosities of both  
638 upper and lower mantle, are within the orange (a-b) and gray bands in (c-h). The red and blue  
639 curves in grey shaded bands (c-h) show the results for lower mantle viscosities of  $10^{22}$  and  $10^{23}$   
640 Pa s respectively with 70 km lithospheric thickness and upper mantle viscosity of  $10^{20}$  Pa s.  
641 There is remarkable agreement between observations and predictions at all of the sites shown, in

642 particular for the timing into and out of the LGM (Extended Data Figs. 6, 7, 8). Of note is the  
643 foraminiferal oxygen isotope based Red Sea data<sup>20</sup> (h) which supports the new GMSL  
644 calculations from the present study within uncertainties (ca. 10 m). The orange band in (h) is  
645 confidence intervals of 95% for the RSL data (light orange) and probability maximum (dark  
646 orange) reported in ref. 20.

647

648

649

650

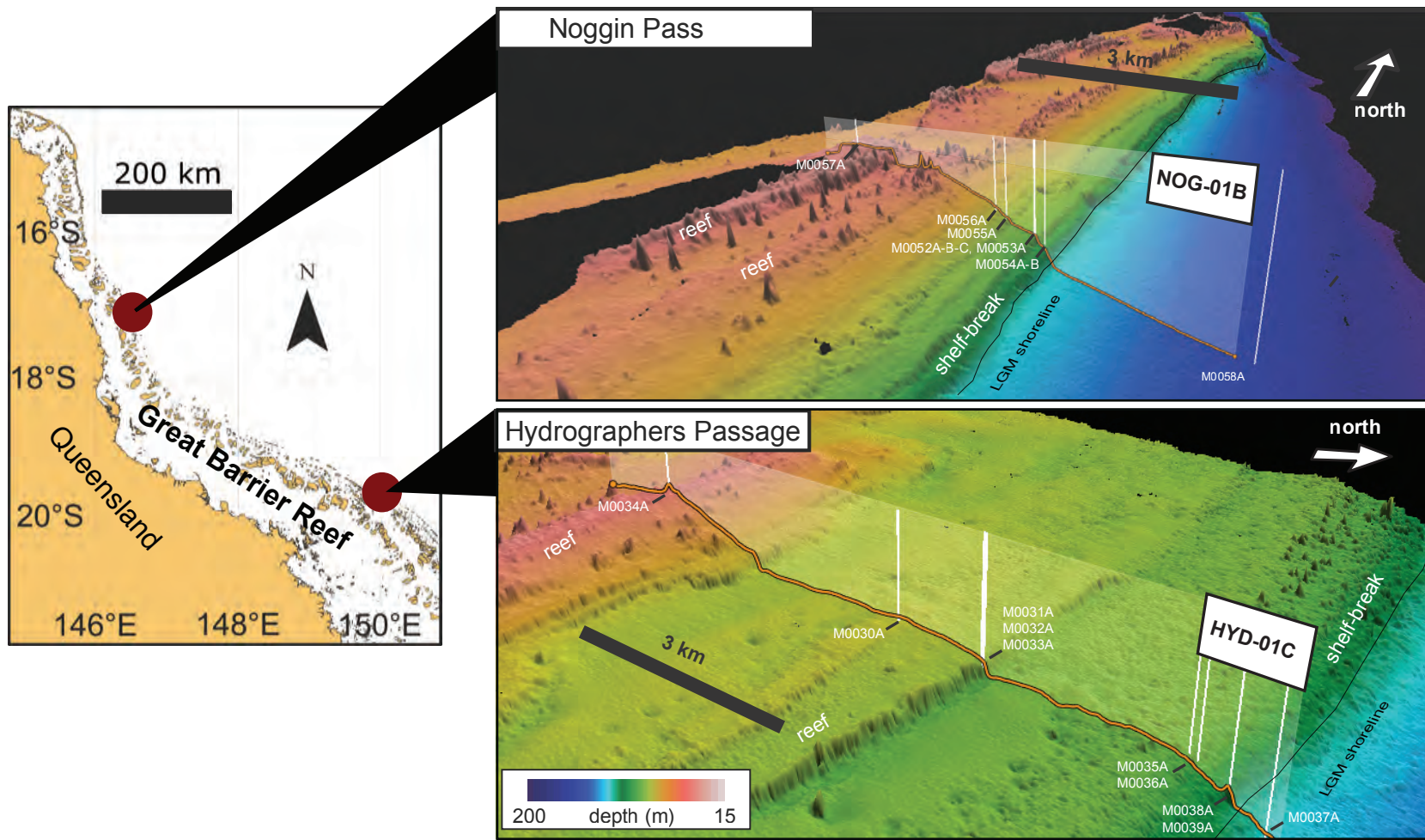
651

652

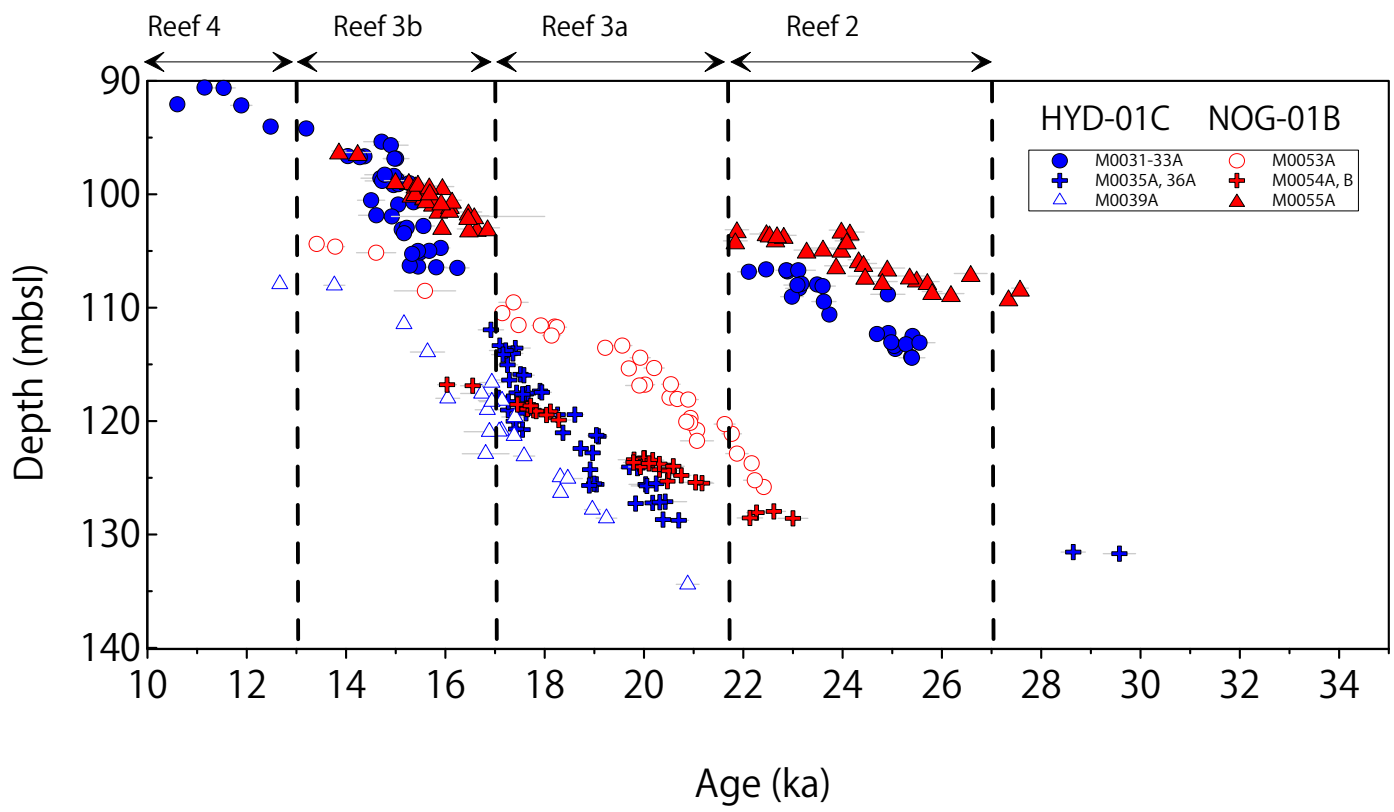
653

654

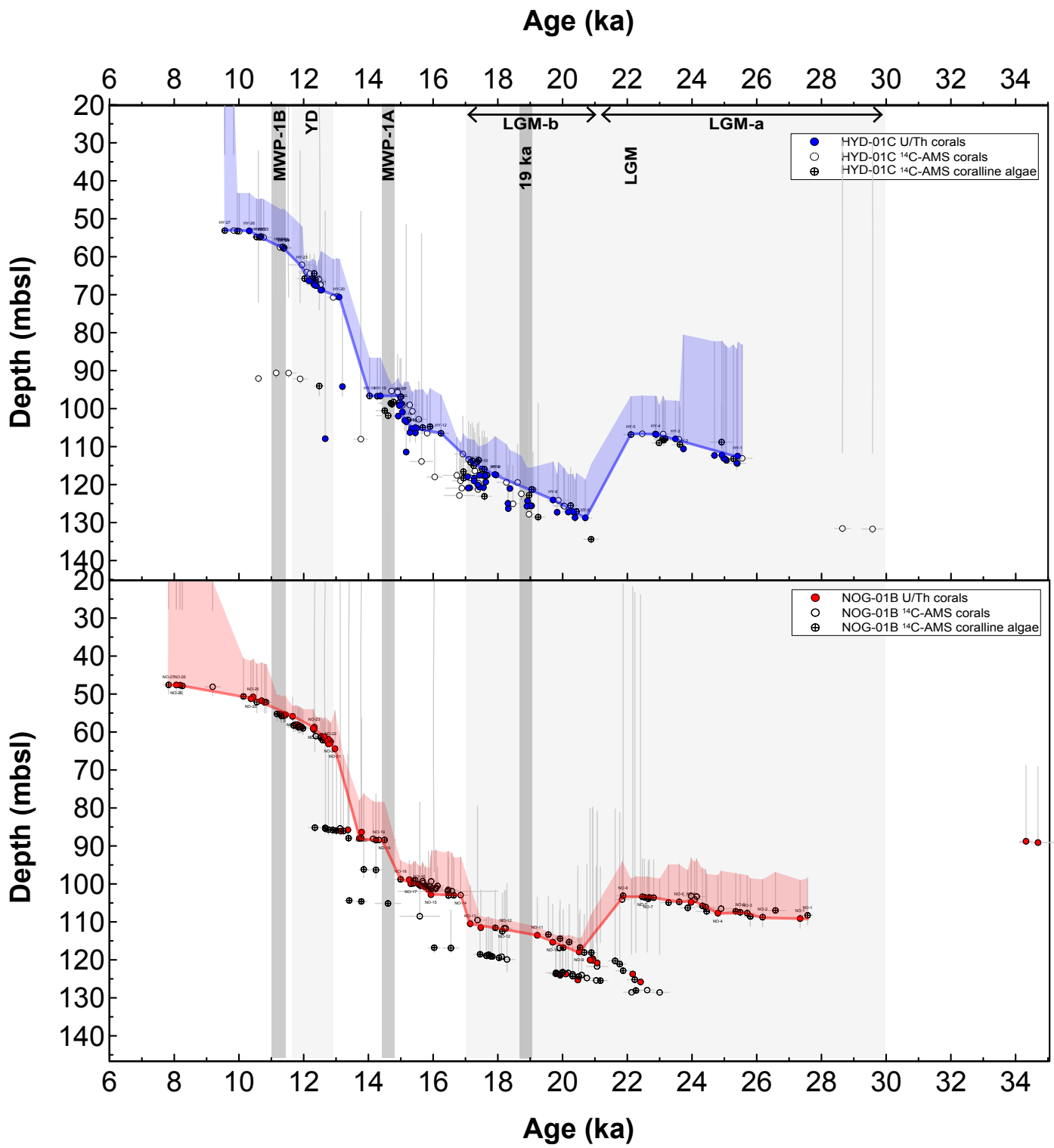
655



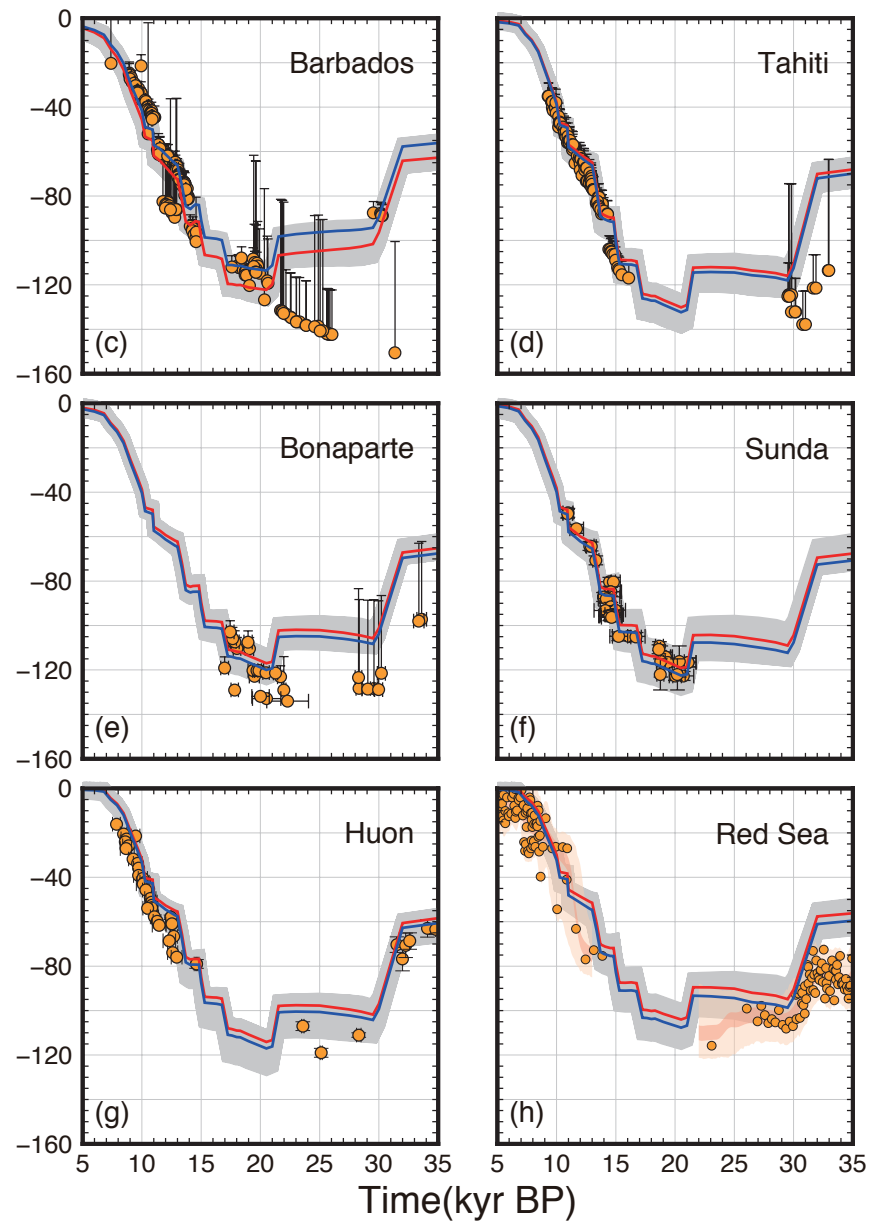
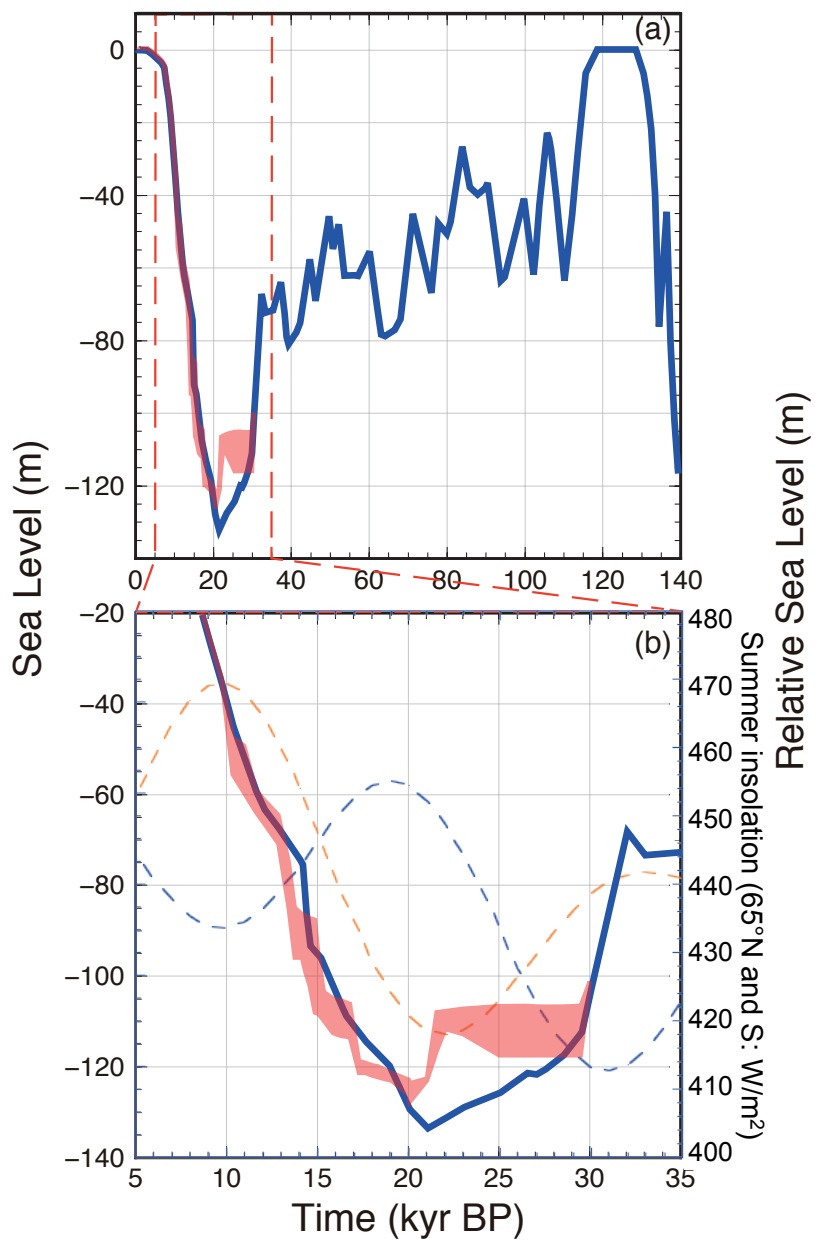
Yokoyama et al. (Fig1)



Yokoyama et al. (Fig2)



Yokoyama et al. (Fig3)



Yokoyama et al. (Fig 4)